SIMULATION OF A ROTOR IN FORWARD FLIGHT USING TOPOLOGY-BASED REFINEMENT OF MULTI-BLOCK STRUCTURED MESHES

H. van der Ven, O.J. Boelens, J.C. Kok,
B.B. Prananta and M.P.C. van Rooij

Flight Physics and Loads Department
Netherlands National Aerospace Laboratory
P.O. Box 90502, 1006 BM Amsterdam
Harmen.van.der.Ven@nlr.nl

Abstract

The simulation of blade-vortex interaction (BVI) for helicopter rotors remains a challenge for Computational Fluid Dynamics (CFD). In the current paper a high-order, block-structured, finite volume flow solver is applied to the well-known HART-II baseline case. A new grid generation algorithm is presented which allows the automatic generation of locally refined meshes in user-specified regions, based on a regular block-structured mesh. The algorithm is used to generate a mesh with a given uniform resolution in the rotor disk area. The convection of the tip vortices is expected to improve on such a mesh. Flow results on both the unrefined and refined mesh confirm this expectation.

Symbols and abbreviations

BVI	Blade-Vortex Interaction
CFD	Computational Fluid Dynamics
NLR	National Aerospace Laboratory
R	rotor radius
$C_N M^2$	normal force coefficient $C_N M^2 = \frac{N}{\frac{1}{2}\rho_\infty a_\infty^2 A}$
N	normal force [N]
ρ_∞	atmospheric air density [kg/m^3]
a_∞	atmospheric speed of sound [m/s]
A	reference area [m^2]
θ_0	collective pitch [°]
θ_{1c}	longitudinal cyclic pitch [°]
θ_{1s}	lateral cyclic pitch [°]
ψ	azimuth angle [°]
Q	Q-criterion: $\Omega^2 - S^2$ [s^{-2}]
S	magnitude of strain rate tensor [s^{-1}]
U_∞	forward rotor speed [m/s]
Ω	magnitude of vorticity [s^{-1}]

1 Introduction

In level helicopter flight there are two regimes with high vibration levels, low speed transition flight and high speed forward flight. The two high vibration regimes translate directly into high operating and maintenance costs. There are three key aerodynamic phenomena which contribute to the vibratory loads: wake induced air loads, compressibility effects, and dynamic stall. The current paper focuses on the accurate resolution of wake-induced air loads using Computational Fluid Dynamics (CFD) techniques.

As summarised in Datta et al. [1], first principles

CFD calculation of the wake is primarily a grid refinement problem. In order to capture the tip vortices the computational mesh must be refined in the vortex regions, which are not known beforehand. The dynamic nature of the wake in forward flight complicates the refinement problem since the vortices change position over time.

With the increase in computing power, there is a tendency in the CFD community to apply simple high-order finite difference schemes on dense Cartesian background meshes and standard second-order finite volume schemes in the neighbourhood of the geometry (Jayaraman et al. [2] and Sankaran et al. [4]). While this method shows impressive vortex capturing capabilities on the background mesh, it has two drawbacks: 1) the numerics are only second order in the proximity of the rotor blades; 2) the Chimera approach requires interpolation of the flow solution between the two types of grid.

At NLR a high-order, block-structured, finite volume flow solver has been developed which maintains its high order of accuracy in the whole of the computational domain (Kok [3]). The main challenge in applying this solver to rotor flow is to obtain a grid resolution similar to the resolution of the background grid used in [2, 4]. Geometrical and topological restrictions normally prevent the generation of a block-structured grid which has a uniform resolution in the rotor wake.

In the current paper a topology-based refinement scheme is presented which allows the generation of such meshes. In the approach, the block topology is refined in such a way that a uniform mesh can be obtained locally without outward radiation of the grid density. This is achieved at a cost: at block boundaries the grid may be irregular. Mesh width ratio's of 2:1 or higher may be present. However, since the block boundaries are still conforming it is possible to devise high-order accurate schemes across such boundaries.

The outline of the report is as follows. Section 2 describes the refinement algorithm for the generation of the appropriate meshes and the discretization scheme on the irregular block interfaces. Section 3 describes the refined mesh for the HART II test case and the simulation results for the refined and unrefined mesh. Finally, in Section 4 conclusions are drawn.

2 Topology-based block-refinement algorithm

2.1 Grid generation algorithm

The multi-block flow solver ENSOLV at NLR allows block-wise refinement of the mesh, where the grid in a block is refined in one or more direction(s). The resulting irregularities at block interfaces, where the ratio of mesh widths may be 2^n:1, can be treated by the finite-volume flow solver in an accurate way. Block-wise refined meshes have the potential of attaining uniform grid spacing in the vortex regions. However, the grids may not be that efficient, since the grid resolution may be too small in some regions. This may happen inside the vortex region for a block with significant stretching: if the coarse cells satisfy the resolution requirement, the fine cells will be too small. It may also happen outside the vortex region when the refined block is only partially contained in the vortex region. These examples show that an efficient grid with block-wise refinement can only be obtained if the topology of the mesh is modified.

The algorithm consists of the following steps:

1. uniform refinement of the block topology to a fixed block size (measured as the number of cells within a block); typically the target block size is 8^3 or 16^3;

2. further topology-refinement of those blocks which are targeted for grid refinement; the subblock topology is such that each grid-refined subblock is as close as possible to the fixed block size used in step 1;

3. based on the user-defined maximum grid irregularity (2:1, 4:1, etc.) blocks bounding the refinement region are targeted for refinement, and step 2 is repeated for those blocks;

4. generate the block grids within the refined topology.

In step 2 a refinement sensor is used which indicates how the grid within a block should be refined. The sensor consists of two parts: 1) the target mesh width; 2) the region where this mesh width should be attained. The target mesh width should be attained for all cells within a block. The refinement region can be specified in different ways:

- distance to a geometric object;
- specification of specific blocks;
- a region described by a simple geometric object such as a sphere, cylinder, or cube.

The algorithm is demonstrated for the NACA0012, using a refinement region defined by the distance to a line segment. This example serves as a illustration of the algorithm only, in Section 3.1 the algorithm will be applied to the BO105 rotor.

The original mesh and topology is shown in Figure 1a. With a specified block size of 8^2, the refined topology of step 1 of the algorithm is shown in Figure 1b. The line segment used to define the refinement region is shown in Figure 1c. A region at a distance of 10% chord to this segment is defined as the refinement region. Within this region a mesh width of 0.001 chord should be attained. Figure 2a shows the refined topology which is the result of step 2 of the algorithm. Note that at this stage the grid has not been refined yet and that some of the blocks in the refined topology consist of a single cell of the original mesh.

Subsequently, the user-defined irregularity is applied. Figure 2b shows the refined topology based on a maximum irregularity of 2:1. In the last step of the algorithm the refined grid is generated, which is shown in Figure 2c.

It is worthy to note that the final topology consists of 982 blocks. Clearly, it is unfeasible to expect from a user to generate such topologies by hand.

2.2 Discretization scheme on irregular block interfaces

At the irregular block interfaces the standard numerical scheme cannot be applied since the cell-centered flow data is not available at the other side of the interface. The flow data is interpolated to the required location in planes parallel to the interface, as shown in Figure 3. The interpolation is performed in computational space, that is, the actual mesh widths are not used as weights in the interpolation, but the weights shown in the figure are used. This is in agreement with the underlying high-order scheme. It should be noted that normal to the interface no interpolation takes place: the planes are considered to be at the right location. This obviously is a crude approximation, but in practice the algorithm is robust, and vortices pass through the interface relatively undisturbed, provided the coarse grid resolution is sufficient.

3 Results

3.1 Grid

For rotor flows the convection of the tip vortices in the wake of the blades is important for the capture of the blade-vortex interaction. As the vortices move through the wake, the easiest way of obtaining a mesh with sufficient resolution in the vortex regions is to uniformly refine the mesh in a cylinder around the rotor blades. So the definition of the refinement region in this case is a cylinder centred at the rotor hub with radius equal to the rotor radius and sufficient height to contain the vortices.

The target mesh width is $0.01R$, where R is the rotor radius. This corresponds to 16% chord, which is on the coarse side.

The original mesh has 13 million cells, the refined mesh has 26 million cells. Figure 4a shows a detail of the original mesh in a horizontal plane through the hub. The same detail of the refined mesh is shown in Figure 4b. The uniform resolution in the wake is clearly visible. The imposed grid regularity of 2:1 is also visible in the resolution outside the rotor disk. Figure 5 shows the refinement in a vertical plane through the hub bisecting the rotor disk between two blades.

Figure 6 demonstrates that the target mesh width is actually obtained in the specified refinement re-

gion. The figure shows the ratio of the maximum mesh width in a cell over the target mesh width. As can be seen the ratio is less than one in the refinement region, demonstrating the correct functioning of the algorithm. The figure also shows that the algorithm is relatively efficient: the region where the target mesh width is attained is not that much bigger than the refinement region.

3.2 Rigid-blade trim

As a pre-cursor computation the rotor is trimmed with rigid blades.[1] The rotor has been trimmed to the experimental values of thrust (3300N), rolling moment (20Nm), and pitching moment (-20Nm). The trimmed pitch controls are $\theta_0 = 3.07°$, $\theta_{1c} = 1.92°$, and $\theta_{1s} = -1.61°$. The obtained thrust is 3630N, 10% higher than the experimental thrust. As the main objective of the current simulation is to investigate the effect of local grid refinement, and not comparison with experiment, the trim is not pursued to higher accuracy. At these trim conditions there is evidence of BVI on the retreating side (see next section), so the conditions are sufficient for the current investigation.

3.3 Flow results

All simulations have been run using the fourth-order accurate finite volume scheme. Simulations have been performed on the original mesh of 13 million elements, and the locally refined mesh of 26 million elements (see Section 3.1 for details). The time step corresponds to 1.0° azimuth for the original mesh, and to 0.5° azimuth for the refined mesh.

Figure 7 shows the instantaneous iso-contour of the Q-criterion for the original mesh. The value of Q is equal to $0.36U_\infty/R$; the vorticity is scaled with $2U_\infty/R$. Figure 8 shows the instantaneous iso-contour of the Q-criterion for the refined mesh at the same values of Q and vorticity. The increase in vortex resolution is evident.

The sectional vertical force coefficient at 87% for the two simulations is shown in Figure 9. The reference area for the force coefficient is equal to the blade chord times the width of the blade section (which consists of the grid faces on the blade intersected by the 87% span plane). The global increase in sectional lift for azimuth angles between 120 and 250 degrees is most probably not caused by the increased spatial resolution, but rather by the smaller time step for the simulation on the refined mesh.

As the blades are assumed rigid, no comparison is made with experiment, which has elastic blades. Nonetheless, the sectional forces show evidence of BVI on the retreating side, at more or less the same location as in the experiment. The BVI resolution improves on the locally refined mesh. This confirms the expectation that uniform meshes in the rotor wake are beneficial for vortex resolution, and hence for the prediction of BVI.

[1] Results with elastic blades will be shown at the conference

4 Conclusions

A new grid generation algorithm for block-refined structured meshes has been presented. The algorithm has been applied to generate a mesh around the HART-II rotor which has uniform resolution in the rotor wake. Assuming rigid blades, the rotor has been trimmed to the experimental conditions. Simulation results are compared for simulation on the unrefined and refined mesh.

The uniform resolution of the refined mesh in the rotor wake improves the resolution of the tip vortices. As a consequence, the prediction of the BVI phenomenon on the retreating side has improved, compared to the simulation on the unrefined mesh.

Acknowledgements

The work described in this paper is partially funded by the EU FP7 IDIHOM project and partially by NLR's programmatic research 'Kennis als Vermogen'.

References

[1] A. Datta, M. Nixon, and I. Chopra. Review of rotor loads prediction with the emergence of rotorcraft CFD. *J. of the American Helicopter Society*, 52 (4):287–317, 2007.

[2] B. Jayaraman, A.M. Wissink, J.W. Lim, M. Potsdam, and A.C.B. Dimanlig. Helios prediction of blade-vortex interaction and wake of the HART II rotor. Technical Report 2012-0714, AIAA, 2012.

[3] J.C. Kok. A high-order low-dispersion symmetry-preserving finite-volume method for compressible flow on curvilinear grids. *J. Comput. Phys.*, 228:6811–6832, 2009.

[4] V. Sankaran, J. Sitaraman, A. Wissink, A. Datta, B. Jayaraman, M. Potsdam, D. Mavripilis, D. O'RBrien, H. Saberi, R. Cheng, N. Hariharan, and R. Strawn. Application of the helios computational platform to rotorcraft flowfields. Technical Report 2010-1230, AIAA, 2010.

[5] B.G. van der Wall. 2nd HCC aeroacoustics rotor test (HART II) Part I: Test documentation. Technical Report IB 111-2003/19, DLR, 2003.

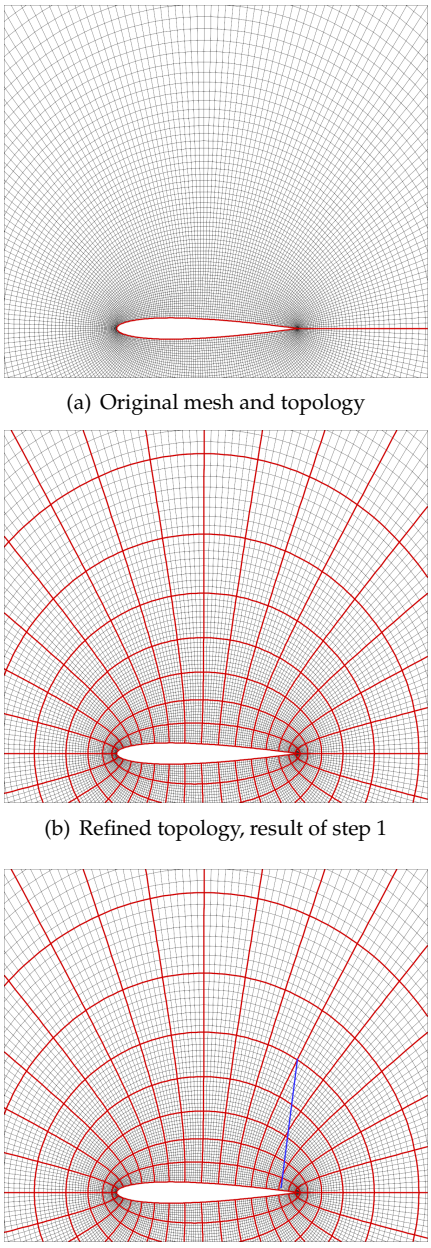

(a) Original mesh and topology

(b) Refined topology, result of step 1

(c) The sensor

Figure 1: Illustration of the grid generation algorithm. Block boundaries are shown in red; grid lines in black; the line segment used in the sensor is shown in blue.

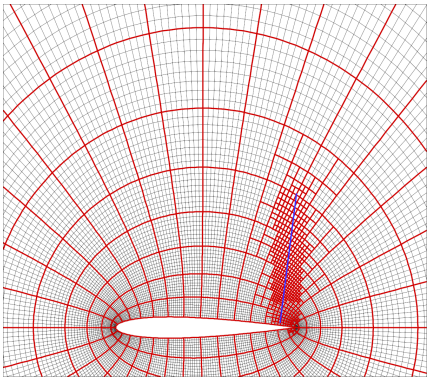

(a) Refined topology, result of step 2

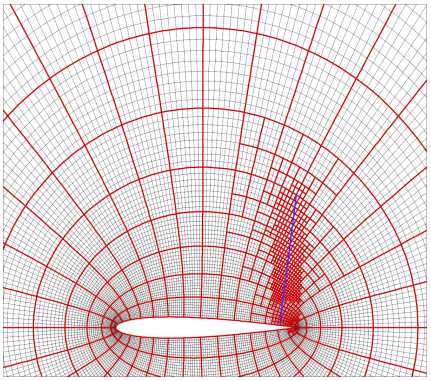

(b) Refined topology, result of step 3

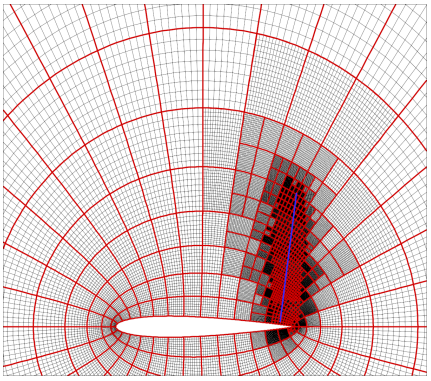

(c) Refined grid, result of step 4

Figure 2: Illustration of the grid generation algorithm. Block boundaries are shown in red; grid lines in black; the line segment used in the sensor is shown in blue.

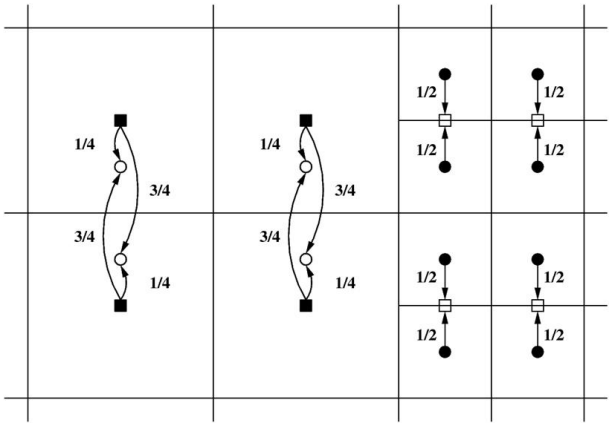

Figure 3: Illustration of the interpolation algorithm at an irregular block interface

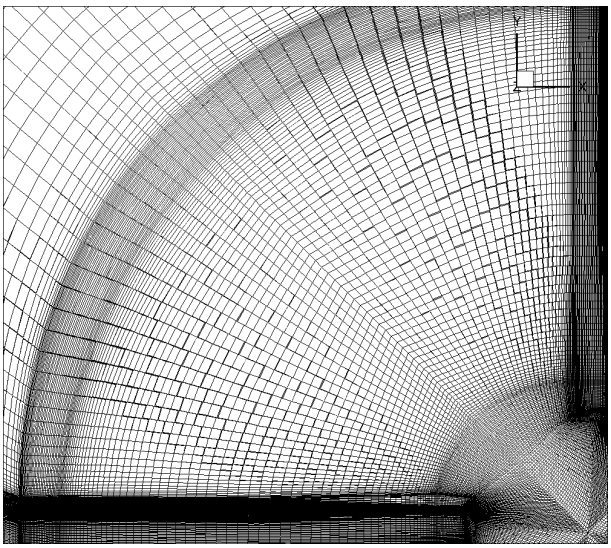

(a) Original mesh

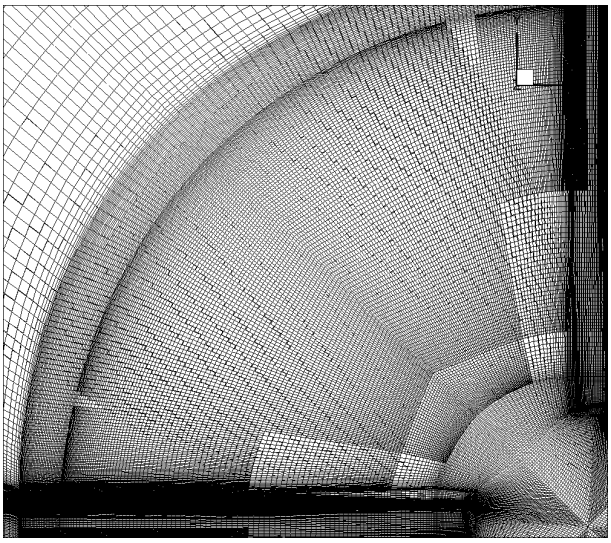

(b) Refined mesh

Figure 4: Original and refined mesh for the BO105 rotor at a horizontal plane through the hub.

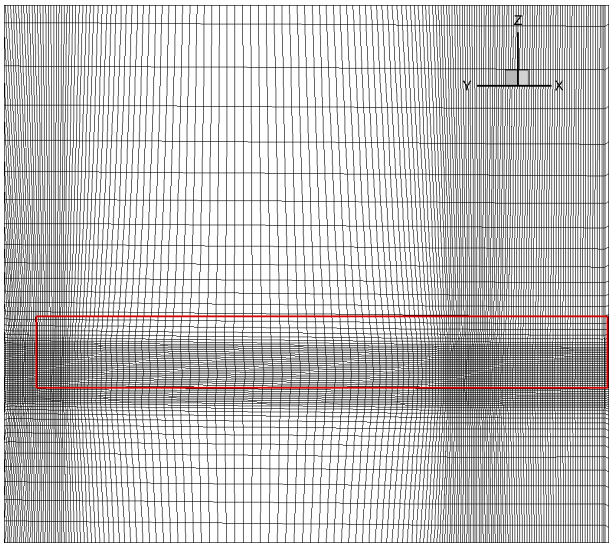

(a) Original mesh

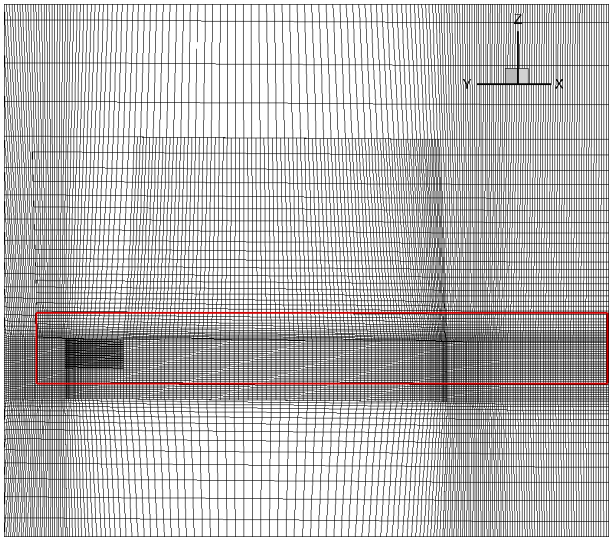

(b) Refined mesh

Figure 5: Original and refined mesh for the BO105 rotor at a vertical plane between two blades. The refinement region is within the red rectangle.

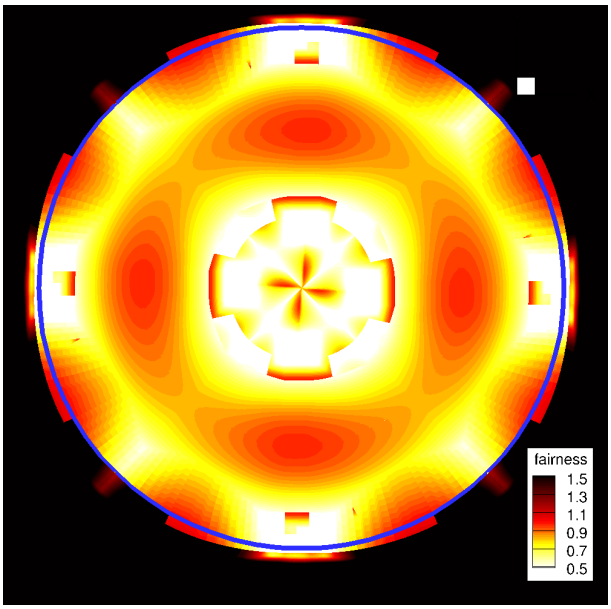

(a) Horizontal plane

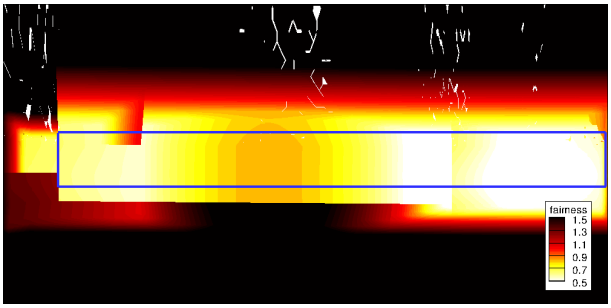

(b) Vertical plane

Figure 6: Ratio of the maximum mesh width in a cell over the target mesh width in the same two planes as in the previous figures. The refinement region is shown in blue.

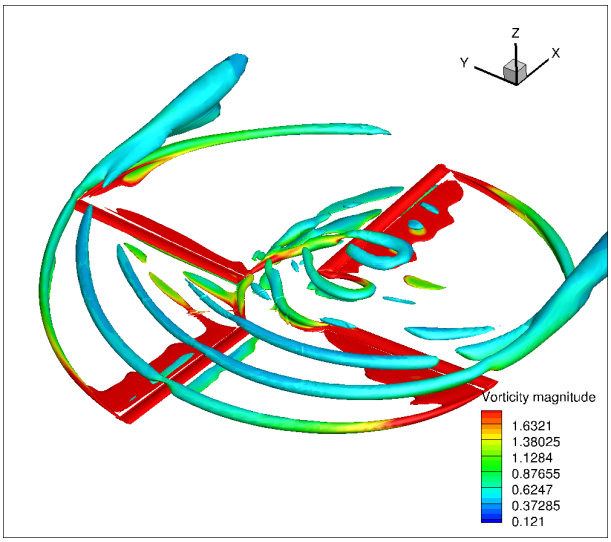

Figure 7: Instantaneous iso-contour of the Q-criterion (blade at 0° azimuth) coloured with vorticity magnitude for the original mesh.

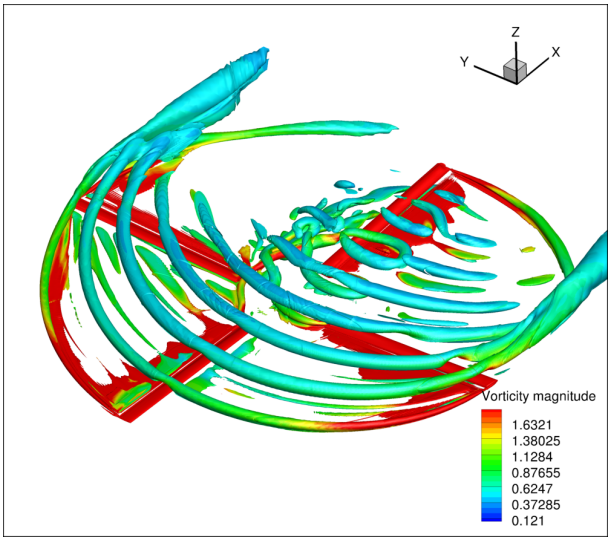

Figure 8: Instantaneous iso-contour of the Q-criterion (blade at 0° azimuth) coloured with vorticity magnitude for the refined mesh.

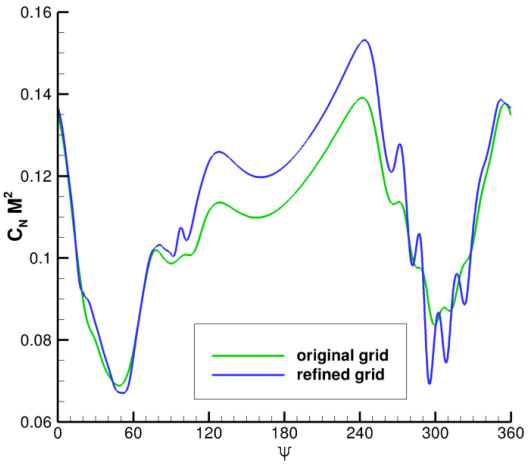

Figure 9: Vertical force coefficient at 87% span. Note that the simulations have been performed for rigid blades.